Transactions, SMiRT-22
San Francisco, California, USA - August 18-23, 2013
Division IX (include assigned division number from I to X)

CRACK INITIATION IN AUSTENITIC STAINLESS STEEL OWING TO CYCLIC THERMAL SHOCKS AND BIAXIAL PRELOAD

Markus Niffenegger[1], Bojan Niceno[2], Medhat Sharabi[2], Koenraad G. F. Janssens[1], Klaus Reichlin[1]

[1] Laboratory for Nuclear Materials, Nuclear Energy and Safety Research, Paul Scherrer Institute, 5232 Villigen, Switzerland
[2] Laboratory for Thermo Hydraulics, Nuclear Energy and Safety Research, Paul Scherrer Institute, 5232 Villigen, Switzerland

ABSTRACT

Specific thermo-hydraulic conditions, e.g. turbulences caused by mixing hot and cold water, may lead to cyclic thermal shocks (CTS) in the primary circuit piping of light water reactors. This may result in crack initiation, possibly followed by crack growth and failure of the component, which is a phenomenon that has been widely investigated. Howbeit, there is still a lack of knowledge concerning the conditions under which the critical turbulences occur, and the exact boundary conditions promoting the development of crack networks have not been revealed till date.

At the Paul Scherrer Institute (PSI) in Switzerland the above questions are addressed by experimental investigations and numerical simulations of the complex fluid dynamics and the thermal stresses induced in the piping material. The overall aim of these investigations is to acquire a better understanding of the governing mechanisms and to improve numerical tools for the prediction of component's lifetime. For the investigation of crack initiation and growth in austenitic stainless steels (ASS) due to CTS, a new thermo-shock facility allows to load test specimens simultaneously with CTS and biaxial mechanical forces under well-defined boundary conditions.

Besides the experimental work, the ongoing numerical modeling concentrates on the simulation of turbulent fluid flow and the concerning temperature fluctuations in mixing tees, the advanced description of cyclic plasticity and the simulation of component failure due to the cyclic thermal shocks.

In this report the ongoing research activities at PSI in the field of thermo-mechanical fatigue and some preliminary results are presented. In particular, a new thermal shock facility allowing cyclic thermal shock experiments on flat surfaces is described. Furthermore, a real T-joint was chosen to demonstrate the performance of the computational tools by comparing measured with calculated temperature fluctuations in the mixing tee, followed by a subsequent lifetime analysis.

INTRODUCTION

Damage has been reported in T-junctions where hot and cold water is mixed, Metzner (2005). In nuclear power plants (NPP) the phenomenon of thermo-mechanical fatigue (TMF) may appear in the low cycle (LCF) or/and in the high cycle fatigue (HCF) regime, and is, referring to NEA/CSNI/R (2005) and OECD, (2006), usually connected with operating transients (LCF, covered by existing rules and codes), stratification due to temperature differences in horizontal tubes (LCF, partially covered by national rules) or mixing of cold and hot water flow, e.g. in T-junctions (LCF and HCF, not anticipated at the design stage and therefore not covered by design rules). In particular CTS, caused by the unstable turbulent flow in cold and hot water mixing streams, is leading to temperature fluctuations at the inner wall of the piping, where the induced thermal stresses may end up in a network of micro cracks (elephant skin). This elephant skin, also called crazing, is characteristic for the biaxial stress/strain state due to thermal shock load, especially if superimposed to other loads, e.g. internal pressure or residual stresses in welded tubes. Although most micro cracks arrest short of approximately 2 millimeters, under certain circumstances, some of them may grow through the wall as reported in several publications e.g. Faidy (2000), Cipiere et

al. (2001, 2002), Hirschberg (2000), Deardorff (2004). Such damage was not anticipated at the design stage but observed in some mixing tees. However, in spite of the common agreement concerning the origin of this damage, the exact conditions responsible for macroscopic failures are still unknown and there is still a need of tools for the reliable prediction of the turbulences, crack initiation and crack growth under operating conditions.

This TMF phenomenon has been widely investigated, e.g. Fissolo et al. (2004) and Haddar et al. (2004), but there is still a lack of knowledge concerning the conditions under which the critical turbulences occur, and concerning the boundary conditions leading to the development of crack networks as well as under what conditions the growth of single cracks may result in the failure of components. In particular the following questions still need to be answered:

- Under which flow conditions do the thermal fluctuations appear? (Thermo-hydraulic problem)?
- What are the critical locations for crack formation in the primary loop of a LWR?
- What are the temperature differences ΔT and frequencies ω of these fluctuations?
- Which conditions (ω, ΔT, mean temperature T_m, pressure) have to be fulfilled for the initiation and growth of thermally induced cracks?
- How deep do these cracks grow? Under what conditions do they arrest?
- What are the differences between different austenitic stainless steels?
- What is the difference between unilateral (hot-cold) and bilateral (cold-hot-cold) thermal shocks?
- What are the reliable mathematical (deterministic and probabilistic) models for fatigue life prediction?

At PSI some of the above questions are addressed within a project called PLiM which is dedicated to the experimental and theoretical investigation of thermo-mechanical fatigue (TMF) owing to CTS, and dedicated to the thermo-hydraulic prediction of turbulent fluid flow leading to these CTS. The overall aim of these investigations is to acquire a better understanding of the governing mechanisms and to improve numerical tools for the prediction of a component's lifetime.

At PSI first CTS experiments were performed on notched ring specimens made from the ASS, partly described by Niffenegger et al. (2009). Some results are summarized below, but the focus in this paper is put on experiments on flat, un-notched and biaxial-mechanically loaded thermo-shock specimens. The aim of these experiments is to mimic real loading conditions with steam and water and to investigate the initiation phase of crack networks on flaw-free surfaces.

For the investigation of crack initiation and growth induced by CTS, PSI's new biaxial thermo-shock facility allows loading test specimens simultaneously with CTS and biaxial mechanical forces under well-defined boundary conditions. In the CTS experiments performed on ASS, the threshold for the ΔTs and applied mechanical stress as well as the number of CTS needed for crack initiation, are under investigation. Furthermore, the new CTS facility also allows investigating the influence of the biaxiality in the preload on the appearance of crack networks (crazing).

Besides the experimental work, the ongoing numerical modeling concentrates on the simulation of turbulent fluid flow and the concerning temperature fluctuations in mixing tees, Kuhn et al. (2010), the advanced description of cyclic plasticity, Janssens (2011) and the simulation of component failure due to the cyclic thermal shocks Janssens et al. (2008).

The investigations show that amplitudes of temperature fluctuations can be predicted with relative ease, using large scale flow simulations such as Unsteady RANS (URANS), Large Eddy Simulations (LES), Very Large Eddy Simulations (VLES), Scale-Adaptive Simulations (SAS). LES simulations were proven to give superior results and were therefore used to analyze the fluid flow in the T-joint.

THERMOSCHOCK EXPERIMENTS ON NOTCHED RING SPECIMENS

Former CTS-experiments were performed by pushing alternatively cold and hot oil on the wall of the bore on notched ring specimens shown in Fig. 1. Two thermal load profiles, shown in Fig. 2, were applied, namely unilateral (hot-cold) and bilateral (cold-hot-cold) shocks. The frequency ($\approx 3 \cdot 10^{-4}$ Hz) of

these CTS was limited by the experimental facility and is far away from that expected in the turbulent flow conditions of mixing tees which are expected to be in the order of 1 to 10 Hz. Furthermore, a larger temperature difference was applied to reduce the experimental time. The transition time for the temperature shocks was about 10 seconds. This applied load corresponds more likely to the conditions in emergency cooling transient than to the cyclic thermal shocks in mixing tees..

In order to determine crack growth the specimens were dismounted after a certain number of CTS. The lengths of the induced cracks were measured in the scanning electron microscope and plotted versus the number of cycles (Fig. 3). Figs. 4-6 show the results for three different low-carbon ASS (AISI 316L, DIN 1.4404) and a Ti- (AISI 321, DIN 1.4541) and Ni-stabilized (AISI 347, DIN 1.4550) austenitic stainless steels (ASS). It can be seen that no significant differences between the three ASS were observed. However, it could be observed that crack initiation and short crack growth for bilateral load was faster than for unilateral load.

The comparison of the experimental results with finite element calculations for the specimens having a notch with radius 0.05 mm and depth of 1mm is shown in Tab. 1. Difficulties appeared in the calculation of the initiation and short crack phase, since the application of fracture mechanics assumes an initial crack which does not exist in the initiation phase. Furthermore, the microstructure (grain size and orientation) is more important in the initiation phase. It is worth mentioning that the sizes of the finite elements were smaller than the grain size in order to model short cracks. Also the cyclic elasto-plastic behavior (kinematic and isotropic softening and hardening) is difficult to consider in the model. Extensive additional fatigue experiments were carried out to determine the cyclic stress-strain loops of the material as a function of the strain amplitude and temperature. The resulting stress-strain loops were fitted in order to consider the complex cyclic plasticity in the finite element calculations.

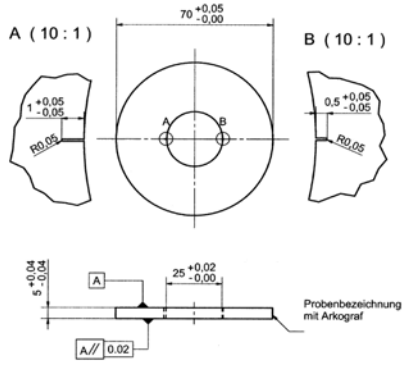

Fig. 1: Notched ring specimen. The inner wall is loaded by cyclic thermo shocks while no mechanical load or constraints are applied.

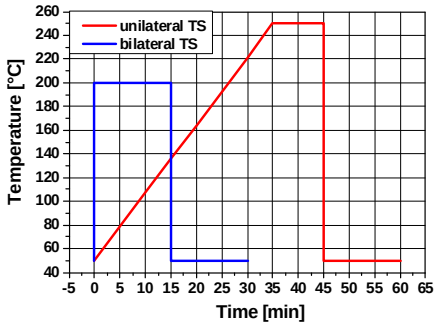

Fig. 2: Uni- and bilateral thermal shocks: Triangular profile ▲ 250 °C - 50 °C and rectangular ▄ 50 °C – 200 °C - 50 °C.

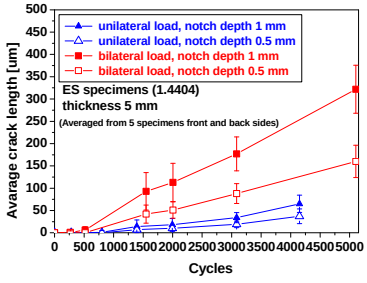

Fig. 3a: Crack length vs number of CTS for DIN 1.4404.

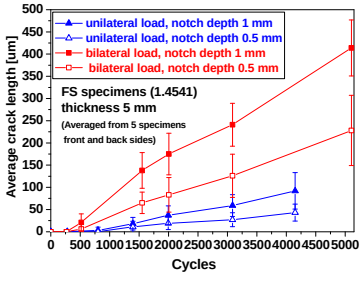

Fig. 3b: Crack length vs number of CTS for DIN 1.4541.

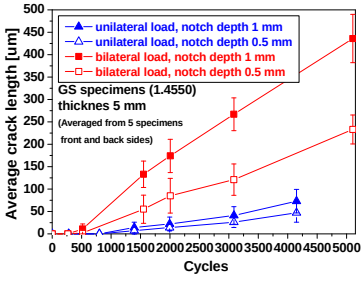

Fig. 3c: Crack length vs number of CTS for DIN 1.4550.

Table 1: Comparison of measured with calculated number of cycles needed for crack initiation

Temperature loading profile (°C)	Steel grade (AISI)	Notch radius (mm)	Maximum stress (MPa)	Strain amplitude (-)	Calculated number of CTS to crackinitiation	Experimentally observed number of CTS to (micro)Crack Initiation
■ 50-200-50	316L	0.05	345	0.0316	254	500
▲250-50	316L	0.05	365	0.0175	574	800

THERMAL SHOCKS ON FLAT SPECIMENS

The New Thermal Shock Facility

In order to overcome the shortcomings mentioned above and to better mimic the real situation in piping, a new test facility shown in Fig. 4 has been built that allows the application of both biaxial mechanical load as well as cyclic thermal shocks on flat (un-notched) cruciform specimens. The size of the test rig for applying the mechanical load is about 60 x 60 cm with a height of 25 cm (without the support and gear engines). A biaxial pull-tension load of maximum 33 kN, applied by means of two asynchronous electro engines, gear drives and spindles, can be applied with a frequency ranging from static load up to 10 Hz. Special bearings at the opposite side of the gear drives allow the compensation of the specimens centre point displacement due to the applied forces in order to avoid any bending on the specimen. The grips are designed to clamp the arms of the specimen and to transmit the force per friction.

The target values (force or displacement) are controlled based on the received instantaneous force/displacement measured by strain gages, piezo transducers and inductive distance sensors. The controller can alternatively be switched to displacement controlled mode. However, most tests were performed in a force controlled mode to allow the compensation of the thermal expansion of specimen and test rig.

In addition to the applied mechanical load the centre part of the cruciform specimen is thermally loaded by cyclic thermal shocks. These shocks are generated by alternating spraying overheated vapor of 460 °C and cold water of 14 °C on a circular area with a diameter of about 10 mm. The frequency of these thermal shocks is typically 1 Hz but may be increased up to 10 Hz. Vapor of 120 °C at 4 bar is produced by an industrial steam generator is fed into a special steam super heater (Fig. 5) in which the vapor is heated up to a temperature of 460 °C while flowing through two concentric Ohm's heating elements and finally injected thru a jet nozzle on the specimen's surface. The jet nozzle is opened and closed, e.g. with a frequency of 1 Hz, by means of a linear motor. A cold water jet is sprayed on the specimen's surface to cause the cold shocks.

A set of new experiments were planned to investigate the crack initiation on flat un-notched specimens under CTS and biaxial mechanical loading. The additional mechanical load allows generating mean stresses similar to those generated by internal pressure or residual stresses which are induced by welding.

Test Specimen

The geometry of the cruciform CTS specimen shown in Fig. 6 has been chosen to allow the application of biaxial forces by means of the four arms. Its shape has been optimized by FE-calculations to achieve a well defined stress state in the center of the specimen. Only the center part of the specimen is loaded by CTS and analyzed. The test specimens are manufactured from warm rolled plates of the low-carbon (AISI 316L, DIN 1.4404) ASS which does not necessarily fulfill the requirements of nuclear installations. The flat center surfaces of the specimen are either polished to achieve a surface quality of N6 in order to allow better analyses of the damage by metallography and scanning electron microscopy or sandblasted in order to achieve more realistic conditions.

Thermal Loading History

Fig. 7 shows the transient temperatures measured by thermocouples at the top center position (in the middle of the hot spot), at a radius of 12 and 50 mm and at radius 5mm at the specimen's back side which is not charged by the heat transfer medium. Fig. 8 shows the surface temperature as a function of time and radial distance from specimen's center. Note that the specimen is additionally heated.

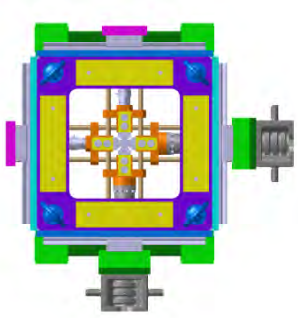

Fig 4: Biaxial load frame for the application of forces up to 33 kN.

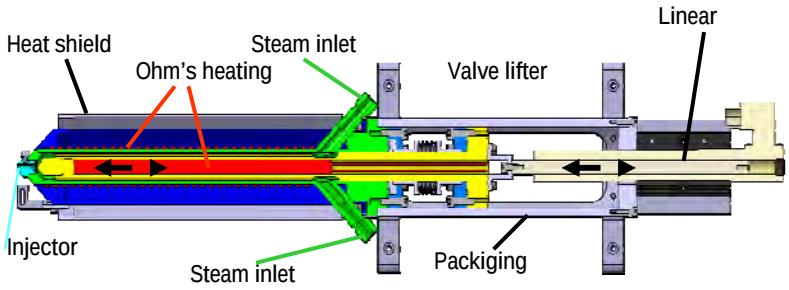

Fig. 5: Steam super heater and injector driven by a linear motor.

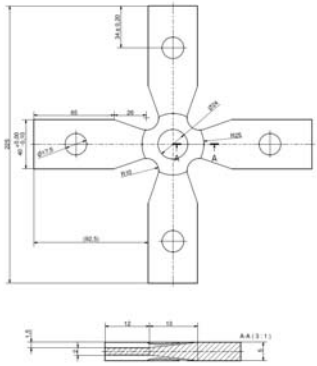

Fig. 6: Cruciform specimen. The center part (radius 5 mm) is loaded by CTS.

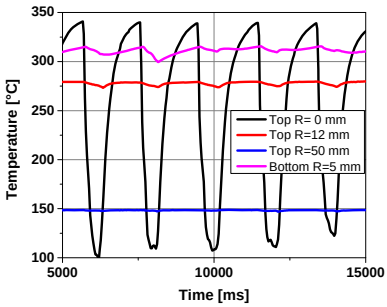

Fig. 7: Temperatures measured with thermocouples on the specimen's surface.

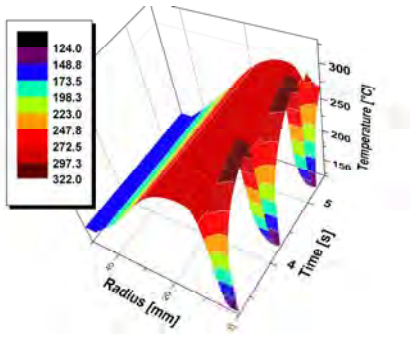

Fig. 8: Temperature profiles vs time and radial distance from specimen's center.

Calculated strains for cyclic thermal load

The CTS experiments were simulated by 3D finite element calculations by first calculating the temperatures followed by stress calculation in which the cyclic plasticity is considered. Since the heat transfer coefficients HTC involved in the CTS are not a priori known they were evaluated in an iterative process in which the HTC was adjusted until the calculated transient temperature profiles were in accord with the measured ones. Note that the HTC depend on temperature and location and that the applied biaxial force of 20 kN corresponds to a static von Mises stress of 130 MPa. Based on the temperature fields calculated with the adjusted HTC and the applied forces, strains and stresses were calculated. The calculated surface temperatures and strains at the specimen's center of the 1 Hz CTS are shown in Fig. 9. Among the plotted total, thermal, elastic and plastic strains the sum of elastic and plastic strains is responsible for the resulting stresses and therefore for the material damage. However, as shown in Fig. 9 the elastic plus plastic strain amplitude caused by a ΔT=200 °C is about 0.12%. The mean von Mises stress in the middle of the specimen, applied by the biaxial forces of 20 kN, shakes down from 60 to 38 kN. If we compare the resulting strain with the life time curve in Fig. 10 of different ASS, we see that in a standard fatigue specimen a strain amplitude of 0.25% is leading to failure after about $N_f=2\cdot10^5$ cycles,

whereas a Δε=0.12% is between the ASME Mean Curve and the ASME III Design Curve. Therefore it can be expected, that the probability for finding cracks in the polished and flat surface is rather small.

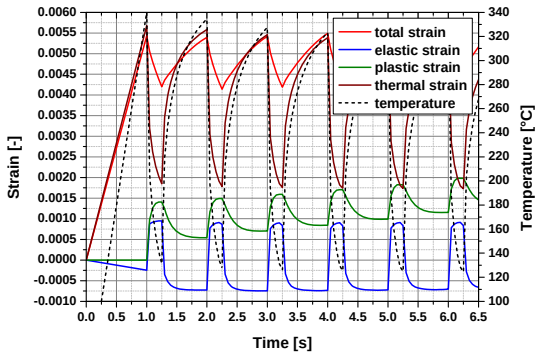

Fig. 9: Cyclic temperatures and strains in the center on the surface of the cruciform biaxially preloaded (20 kN) flat 5 mm thick specimen.

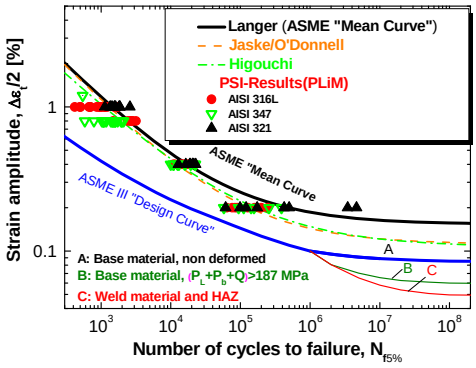

Fig. 10: Life time curves for austenitic stainless steels, own results labeled with symbols.

Results from cyclic thermo-shock experiments

A set of CTS experiments with the loading parameters described above were performed up to a certain number of cycles and analyzed by metallographic investigations and scanning microscopy. Figures 11a to 11f show the change of specimen's surface from zero to $223 \cdot 10^3$ and for $385 \cdot 10^3$ CTS at the specimen's surface (in the center). A crack network was already observed after $223 \cdot 10^3$ CTS which is shown in Figs. 11b and 11c. The Figures 11d to 11f show the hot spot with the crack network at the center of the sand-blasted specimen after $385 \cdot 10^3$ CTS with different amplifications. No cracks were found yet in the specimens having a polished surface.

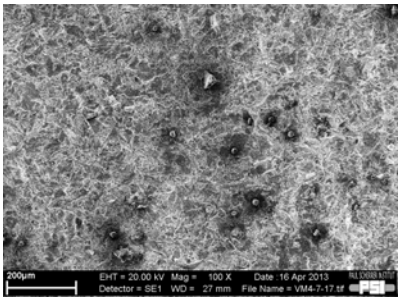

Fig. 11a: Original state (0 CTS) top side surface.

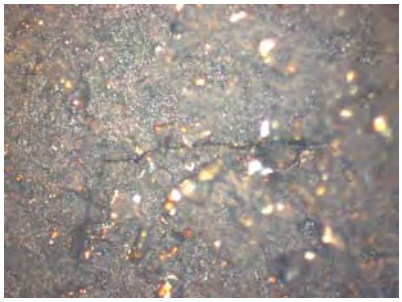

Fig. 11b: Crack network after $223 \cdot 10^3$ CTS top side surface.

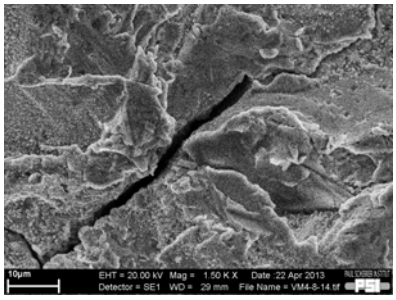

Fig. 11c: Crack network after $223 \cdot 10^3$ CTS top side surface.

Fig. 11d: Crack network inside the hot spot after $525 \cdot 10^3$ CTS.

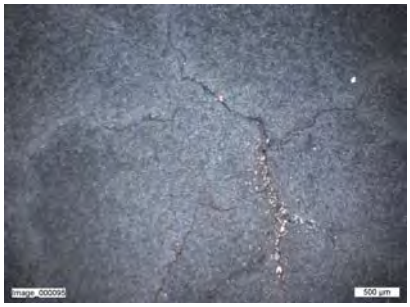

Fig. 11e: Crack network after $525 \cdot 10^3$ cycles top side surface.

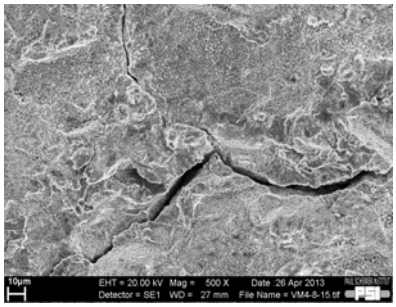

Fig. 11f: Crack network after $525 \cdot 10^3$ CTS.

LIFETIME ASSESSMENT OF A T-JOINT

The performance of the developed computational tools is demonstrated by means of the lifetime assessment of a real T-joint. Therefore CFD calculations were applied to calculate the temperature fluctuations in the mixing tee for steady state and transient operational conditions. The calculated temperatures were compared with measured ones and transferred to the finite element code ABAQUS for the stress calculation. The lifetime assessment is based on the calculated stress variation.

Computational Fluid Dynamics in a T-joint

A real T-junction shown in Fig.12 was studied. It is composed of two circular pipes intersecting at a right angle. The main pipe has a diameter of 270 mm and the branch pipe has a diameter of 68.4 mm and oriented downward. The material for the main pipe is Kesselblech II and the wall thickness is 27 mm while the branch pipe is made of CK 22 and having thickness gradually decreasing to 10.3 mm. A protection plate is welded to the T-junction intersection. This provides a barrier to attenuate the temperature fluctuations, induced by the highly turbulent mixing flow. The protection plate is provided with two holes to equalize the pressure in both sides and thereby mechanical stresses due to pressure differences are avoided.

In steady state operation of the nuclear reactor, a small part of the condensate (24 t/h) is passed through the reactor water purification system, in order to keep the high quality of water flowing through the reactor recirculation system. This purified water is remixed again with main stream (1000 t/h) as it passes through the mixing tee. They have then different temperatures and the turbulence induced temperature fluctuations, which need to be investigated with CFD simulations, can provoke problems of thermal fatigue. On the other hand for the start-up there is not that large amount of condensate and the flow rate through the main pipe is about 0.8 t/h. In addition, only one, out of two water purification systems, is working giving a flow rate of 12 t/h in the branch pipe. During the transient operation the mass flow rate in the main pipe shows oscillations with peaks reaching 10 and 32 t/h. The inlet temperature of the branch pipe is about 180^{o}C and in the main pipe it changes between 30^{o}C and 48^{o}C. The operating pressure oscillates between 10 and 70 bar. Table 2 summarizes the conditions considered in the CFD simulations. This includes the steady state operation, and three different conditions that are encountered during the transient. The temperature difference for the steady state conditions represented by case 1 is only five degrees, and therefore may be not relevant for the study of thermal fatigue, while the maximum difference for the other cases is 150 ^{o}C for the premixed water streams. Also, high temperature fluctuations are expected to occur in the fluid and in the solid regions with amplitudes and frequencies which can lead to cyclic thermal shocks. The tee section is isolated, so heat losses to the environment are negligible. The Reynolds number at the inlet of the main pipe changes considerably between the cases, being in the laminar range for case 3 and becomes too high for case 1. Among the different analysed dynamic conditions of the mixing process, only selected results for case 4 are presented in this report.

LES models and results

LES study for case 4 of Table 1 is briefly presented below. The calculations are three dimensional unsteady and conducted using the ANSYS Fluent 13.0 commercial code. The subgrid scale WALE model is used to model the stresses resulting from filtering operations. This model is designed to produce correct near wall behaviour for wall bounded flows and in addition, it predicts zero turbulent viscosity for laminar regions in the flow domain. This is particularly important for some of the cases under investigation because of the very low Reynolds number at the inlet of the main pipe which gives rise to laminar flow regions, leading to incorrectly assigned high values of turbulent viscosity. The second order central difference scheme is used to discretize the diffusive and convective terms in the momentum equations. The time step used in the simulation is 5×10^{-4} s. The calculations are run for 150 s physical

time. The first 70 s are used to reach statistically steady state conditions and the statistics are gathered over the remaining period. Monitoring of averaged quantities with progression of time, show that the chosen time frames are adequate to produce turbulent statistics independent of the selected frame sizes. Figure 13 shows a snapshot of the instantaneous temperature fields and the location for monitoring points P1 and P30. The temperature variations are very noisy showing temperature difference of 50 K between the minimum and the maximum indicating intensive turbulence activities as shown in Fig. 14 for point P1. The instantaneous temperature field shows hot turbulent structures at the upper wall of the main pipe due to the effect of jet impingement.

The simulations showed meaningful results about the physics of the flow. When the Reynolds number of the flow in the main pipe was much higher than that for the branch pipe, the mixing zone was confined and the secondary flow was drained parallel to the down wall of the main pipe. On the other hand, for cases where the Reynolds number of the main pipe was much lower compared to the Reynolds number in the branch pipe, the branch pipe flow penetrated deeply in the main pipe and directly impinged its upper wall producing complicated flow pattern and intensive mixing.

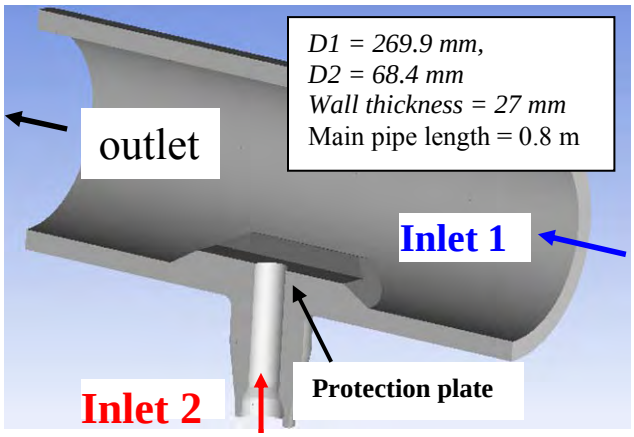

Fig. 12: 3D model of the T-joint

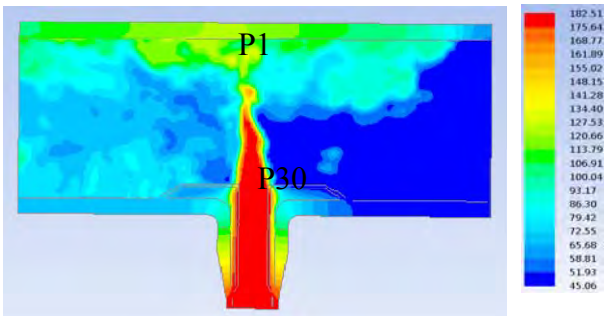

Fig. 13: Snapshot of temperature distribution

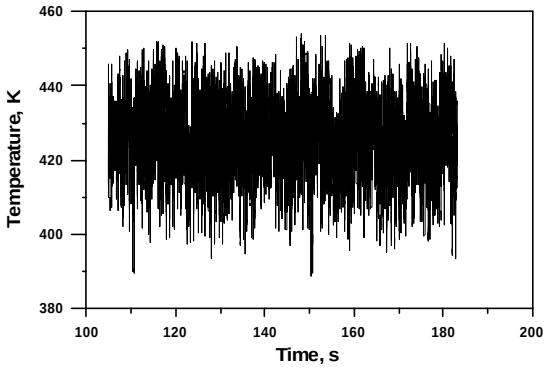

Fig. 14: Temperatures at point P1 vs time.

Table 2: Boundary conditions for the calculated operating conditions.

Parameter	Case 1	Case 2	Case 3	Case 4
m1, t/h	1000	0.8	10	32
m2, t/h	24	12	12	12
Re1	9.3×106	1315	2.3×104	7.4×105
Re2	8.8×105	4.1×105	4.1×105	4.1×105
V1, m/s	5.54	0.004	0.045	0.156
V2, m/s	2.05	1.018	1.018	1.018
T1, oC	194	30	48	48
T2, oC	189	180	180	180
P, bar	76	25	70	25

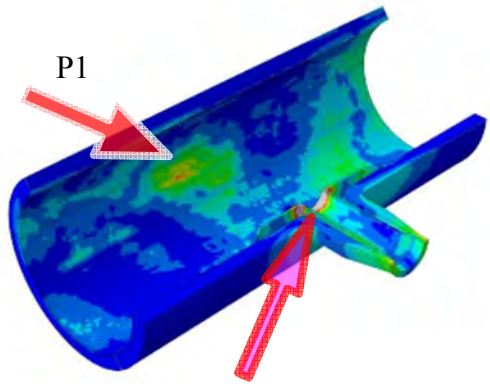

Areas of most severe stress transients in the main pipe

Fig. 15: Von Mises stresses (Snapshot).

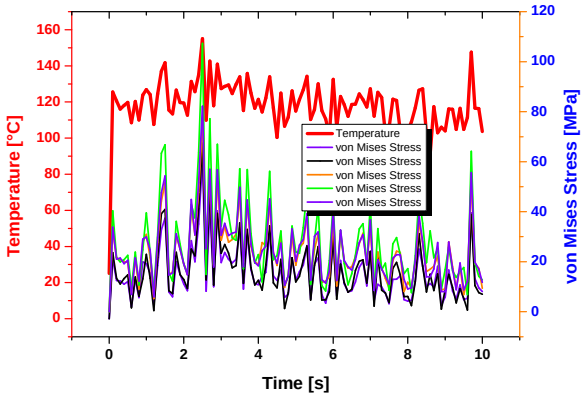

Fig. 16: Von Mises stress and temperature at P1 vs time.

Stress-strain calculations

Stresses based on the calculated temperature fluctuations were calculated with the finite element code Abaqus for the steady state (constant flow rates) case 4. The pipe specifications are given in Tab. 3. Maximal stress amplitudes were calculated in the thermo sleeve (P30) and in the inner wall at the opposite side (P1). Fig. 15 shows the stress distribution at a certain time were maximum values were calculated, whereas in Fig. 16 the variation of the von Mises stress at different points in the vicinity of P30 is plotted for a time period of 10 seconds. It can be seen that most stresses are below 60 MPa while extreme peaks up to 110 MPa were calculated. Fig 16 also shows the temperature fluctuations at P1 calculated by CFD.

Tab. 3: Pipe geometry and material properties

Diameter	inner [mm]	Outer [mm]	Material	Temperature [°C]	E-modulus [GPa]	Mean lin. therm. exp. coefficient [10^{-6} K^{-1}]
Main Feed	269.9	323.9	ASTM A106 Grade B	20 100 200 300 400	210 205 198 192	 12.5 13 13.6 14.1
RCIC/RWCU	68.4	89.0	Ck22 N			
Nozzle	75.0	120.0	ASTM A106 Grade B			

CONCLUSIONS

Both cyclic thermal shock experiments on notched ring specimens and on flat cruciform specimens using a new thermal shock facility are presented. The later experiments are more realistic, i.e. representing the conditions in piping of LWR's. Whereas cracks were induced in the notched ring specimens, it was rather difficult to induce cracks in the polished and un-notched biaxially loaded cruciform specimens by the applied CTS with a ΔT=200 °C. This is in agreement with the expectations resulting from strains calculated with the FEM. However, if the surface were sandblasted a crack network developed within 200'000 cycles.

Large Eddy Simulations performed to calculate the turbulent mixing of cold and hot water in a real T-joint, followed by a stress calculation provided realistic results and the performance of the developed software tool was demonstrated.

Further investigations are needed to systematically investigate combined loading effects.

ACKNOWLEDGEMENTS

We thank Mr. Patrick Simon and Mr. Hans Kottmann for their technical assistance, swissnuclear is acknowledged for founding the PliM project (swissnuclear contract No 1310).

REFERENCES

Cipiere, M.F., Le Duff, J.A. (2001). "Thermal fatigue experience in French piping, influence of surface condition and weld local geometry," Document IIW-XII-1891, Ljubljana, Slovenia.

Cipiere, M.F., Goltrant, O. (2002). "Circuit RRA N4, Incident de Civaux 1," Fontevraud 5, Volume 2, pages 875-882, 23-27.

Deardorff, A. et. al. (2004)." A Survey of Current US Nuclear Plant Fatigue Issues, International Conference on Fatigue of Reactor Components," Seville, Spain, 4-6.

Faidy, C. (2000). "Thermal fatigue in French RHR systems," International conference on fatigue of reactor components, Int. Conf. on Fatigue of Reactor Components, July 31–August 2, 2000.Napa.

Fissolo, A., Maillot, V., Degallaix, G., Degallaix, S., Haddar, N., Roux, J.L., Stephan, J.M., Amzallag, C., Bouchet, F. (2004). "Multiple cracking under thermal fatigue." La Revue Metall., 101 (12), 1087–1099.

Haddar, N., Fissolo A. (2004), "2d simulation of the initiation and propagation of crack array under thermal fatigue," Nucl. Eng. Des. 235, 864–945.

Hirschberg, P.(2000). "Opearting experience regarding thermal fatigue of un-isolable piping connected to PWR reactor coolant systems," International Conference on Fatigue of Reactor Components, Napa. July 31-August 2,

Janssens K. G. F. (2011), "Case study of the applicability of cyclic hardening material descriptions in finite element simulation of cyclic thermal shocks," Fat. Fract. Eng. Mater. Struct. Vol 34, Issue 8, pp. 562-572.

Janssens K.G.F., Niffenegger M. and Reichlin K. (2008) "A computational analysis of cyclic thermal shock induced elasto-plastic ratcheting," Nucl. Eng. Des. 239, 36-44.

Kuhn, S., Braillard, 0., Ničeno, B., Prasser, H-M. (2010). "Computational study of conjugate heat transfer in T-junctions," Nucl. Eng. Des. Vol. 240, Issue 6, 1548-1557.

Metzner, K.-J., Wilke, U. (2005), "European THERFAT project—thermal fatigue evaluation of piping system Tee-connections," Nucl. Eng. Des. 235, 473–484.

NEA/CSNI/R(2005)8, "Thermal cycling in LWR components in OECD-NEA member countries", NEA/CSNI/R(2005)8, July 2005.

Niffenegger M., Janssens K.G.F. & Reichlin K. (2009), "Experimental and Numerical Investigation of Cyclic Thermal Shock at the Paul Scherrer Institute", 20th International Conference on Structural Mechanics in Reactor Technology (SMiRT-20), Espoo, Finland, Augus 9-14, 2009

OECD, (2006). "Nuclear power plant operating experiences from the IAEA/NEA incident reporting system 2002–2005. Tech. Rep. NEA No. 6150, OECD Nuclear Energy Agency.